SIMULATION OF UPPER LAYER BIOCHEMICAL STRUCTURE IN THE BLACK SEA

T. OGUZ[1], H. DUCKLOW[2], E.A. SHUSHKINA[3], P. MALANOTTE-RIZZOLI[4], S. TUGRUL[1], L.P. LEBEDEVA[3] .

[1] *Middle East Technical University, Institute of Marine Sciences, Erdemli, Icel, TURKEY*
[2] *Virginia Institute of Marine Sciences, The College of William and Mary, Gloucester Point, VA, USA*
[3] *P.P. Shirshov Institute of Oceanology, Russian Academy of Sciences, Moscow, RUSSIA*
[4] *Massachusetts Institute of Technology, Department of Earth, Atmospheric and Planetary Sciences, Cambridge, MA, USA*

Abstract: The processes governing the biogeochemical structure of the upper layer water column in the central Black Sea are studied using a one-dimensional coupled physical-biogeochemical model. It is an extention of the previous models (Oguz, et al., 1996; 1997) including the oxygen dynamics and its coupling with the plankton production, particulate matter decomposition and nitrogen transformation, a simplified representation of the microbial loop involving dissolved organic matter generation and bacterial production, as well as the denitrification and hydrogen sulphide oxidation processes. The model thus considers dynamically a fully coupled system of the processes taking place at the euphotic zone, the oxycline, suboxic and anoxic layers. The pelagic food web is represented by two groups of phytoplankton (diatoms and flagellates), three size groups of zooplankton (microzooplankton, mesozooplankton and macrozooplankton). The macrozooplankton group represents essentially a

L.I. Ivanov and T. Oguz (eds.), Ecosystem Modeling as a Management Tool for the Black Sea, Vol. 2, 257-299.

particular gelatinous species group called the medusae "*Aurelia aurita*".

The model simulations reproduce reasonably well the observed annual plankton structure involving a series of successive phytoplankton and zooplankton peaks over the year. In the presence of medusae, the yearly phytoplankton distribution possesses more pronounced summer bloom structures due to stronger "top-down" control of these gelatinous carnivores. The position of the nitrate maximum is shown to be intimately related with the location of the onset of trace level oxygen concentrations as they control the lower limit of the nitrification and the onset of the denitrification in the water column. The model successfully simulates the observed seasonal and vertical variations of the dissolved oxygen in response to its atmospheric and photosythetic productions, and losses during the particulate matter decomposition and nitrogen transformations. The simulations support the presence of an oxygen deficient zone (the so-called the Suboxic Layer) below the 15.6 sigma-t level within the interior Black Sea. The upper boundary of the suboxic layer varies depending on the two opposing mechanisms; the oxygen consumption in the remineralization and nitrification and the ventilation associated with the vertical diffusive transport from the oxycline. Its lower boundary always coincides with the vanishing H_2S concentrations near the 16.2 sigma-t level. In the case of complete oxygenation of this zone, the SOL disappers all together as the positions of vanishing oxygen and H_2S concentrations converge to a common point, implying that their overlapping is not possible under the realistic oxidation rates.

1. Introduction

The Black Sea possesses a distinct vertical biochemical structure representing major characteristic features of the oxygen deficient pelagic waters of the world's oceans. As compared with the Cariaco Trench region, the Eastern Tropical North Pacific and the Arabian Sea, main vertical variations of the biochemical elements are confined within the strongly stratified shallow upper layer of about 100 m. There, the density changes are on the order of 5 kg/m^3 varying from $\sigma_t \sim 11.0$ at the surface to $\sigma_t \sim 16.0$ kg/m^3 at 100 m depth. Four biochemically distinct layers are identified here (Fig. 1). The uppermost part of the water column is covered by a shallow euphotic zone (i.e. from the free surface to the depth of 1% light level) with a maximum thickness of nearly 50 m. This is the layer of active planktonic processes (e.g uptake, grazing, mortality, microbial loop, etc.). This layer is also characterized by high oxygen concentrations of the order of 300 μM. Most of the sinking particles are remineralized within the euphotic layer and the subsequent 20-30 m part of the aphotic zone. As will be demonstrated by our numerical experiments in the following sections, the latter region of active particulate organic material degradation also coincides with intense oxygen consumption and efficient nitrogen cycling, as suggested by the rapid variations in the oxygen and nitrate concentrations (Fig. 1). At the base of this so-called "oxycline" / "upper nitracline" zone, the oxygen concentration reduces to about 10 μM limit whereas the nitrate concentration increases to around 6-8 μM.

At slightly deeper and oxygen deficient part of the water column, organic matter decomposition proceeds via the denitrification. This results in formation of the "lower nitracline" zone with sharp decrease of nitrate concentrations to their trace level values ($\sim 0.1 \mu M$) at a thickness of about 30-40 m below the peak values. This layer is called the "suboxic layer (SOL)", named after the R.V Knorr measurements carried out during the summer 1988 (Murray et al., 1989). The suboxic zone is followed by the deep anoxic layer of hydrogen sulphide (H_2S) and ammonium (NH_4) pools. The boundary between the suboxic and anoxic layers involves a series of complicated redox processes (Murray et al., 1995; Rozanov, 1996), which are mostly unexplored and await further modeling and observational studies. As shown in Fig. 1, it is customary to identify positions of all these characteristic features of the biogeochemical structure using density as the vertical coordinate. These features conform generally along the fixed density levels even though they might be situated regionally at different depths (Vinogradov and Nalbandov, 1990; Tugrul et al, 1992; Saydam et al., 1993).

The pumpcasting measurements performed during the R.V. Knorr measurements identified the suboxic layer by concentrations less than 5 μM in oxygen and 1 μM in sulphide. This was contrary to some observations in which the dissolved oxygen up to 10 μM concentrations were observed within the anoxic layer (Faschuk, et al., 1990; Vinogradov and Nalbandov, 1990) suggesting that the dissolved oxygen and H_2S can coexist together. Later observations carried out by Turkish and Ukranian oceanographers (Basturk et al., 1994 and 1997; Buesseler et al., 1994; Eremeev, 1996) support the presence of the suboxic layer, even though the methodology they used were not as accurate as the

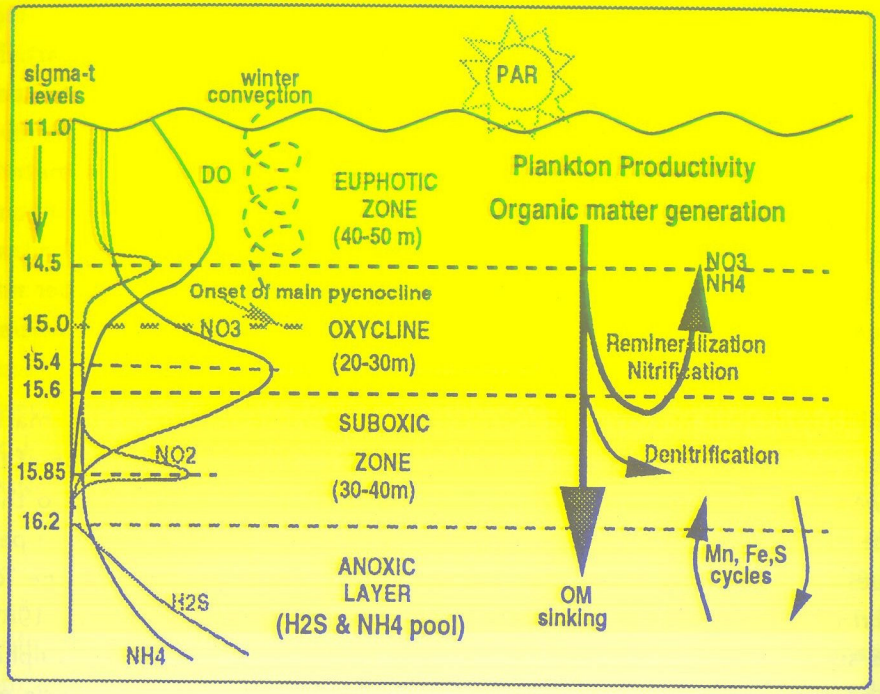

Figure 1: *Schematic diagram of the biogeochemical structure of the upper layer water column in the Black Sea*

pump cast technique employed in the Knorr surveys. They are mostly representative of the summer conditions with almost no reliable data for the winter. Therefore, it is still an unexplored question whether the suboxic layer maintains itself throughout the year or is subject to temporal changes in terms of its characteristics and thickness. It is also not clear whether or not the suboxic and co-existence layers are two different modes of the system under different conditions and seasons. The relative roles of nitrification-denitrification and H_2S oxidation processes also need to be explored for understanding the formation and maintenance of this layer.

The description of the biogeochemical structure given above was based on a purely qualitative basis inferred from the available observations. A comprehensive model providing a quantitative description of the overall biogeochemical structure of the system is not yet available for the Black Sea. The recent modeling studies given by Oguz et al. (1996, 1997) were concentrated mainly on the

simulation of annual plankton production and nitrogen cycling within the euphotic and oxycline/upper nitracline zones. In this context, a five compartment model comprising single groups of phytoplankton and zooplankton, detritus, ammonium and nitrate was first developed by Oguz et al. (1996). It was later extended to a slightly more complex form (Oguz et al., 1997) by distinguishing two major classes of phytoplankton species (diatoms and flagellates) and two dominant zooplankton size groups (micro and meso zooplankton). These models, for simplicity, included neither the microbial loop nor biogeochemical processes in the suboxic-anoxic waters of the Black Sea. They also did not incorporate explicitely the increasing role of gelatinous carnivores (e.g. Aurelia aurita, Mnemiopsis leidyi) in the pelagic food web. These models should therefore be regarded to represent the conditions prior to major ecosystem changes took place in the Black Sea during the last two decades.

The nitrogen and sulfur cycles across the oxic-anoxic interface region have been recently modeled by Yakushev and Neretin (1997). This model is restricted only to the interface region and therefore decoupled from the euphotic zone processes. It is forced from the upper boundary (taken at 50 m depth corresponding approximately to the base of the euphotic zone) by a constant dissolved organic matter concentration, and tuned to study summer conditions instead of a complete annual cycle. As opposed to the oxygen and sulphide depleted suboxic zone, simulations show overlapping dissolved oxygen and sulphide concentrations of less than 10 μM in the region between oxygenated waters and the anoxic pool. No dynamical reasoning, however, is provided for the coexistence of dissolved oxygen and sulphide in the same layer.

In the present work, we elaborate the existing models given in Oguz et al. (1996, 1997) by including (i) an additional macrozooplankton compartment representing specifically the medusae in the food web, (ii) a simple representation of the microbial loop involving bacterial dynamics and dissolved organic material production, (iii) oxygen dynamics, and its role in the processes of particulate matter decomposition and nitrogen transformations, (iv) denitrification and a simplified version of the hydrogen sulphide oxidation processes in the suboxic zone. With these modifications, the model allows for a more complete description of the vertical biogeochemical processes and structure, including some redox processes near the suboxic-anoxic interface. The major objective of the present study is then to simulate the biogeochemical structure

of the interior Black Sea upper layer water column above the anoxic layer, and to provide a quantitative basis for the observations. Albeit the simplicity of the model dynamics and specification of fairly general and idealized initial/boundary conditions, the model will be shown to reproduce most of the observed features of the system and hence might provide a useful tool for understanding functioning of the biogeochemical processes in the Black Sea.

The paper is organized as follows. Section 2 describes the model formulation of the biological interactions with the assumptions and idealizations made as well as the boundary and initial conditions prescribed. Section 3 describes results of the numerical experiments and their consistency with the observed data. Here, the overall annual plankton structure within the euphotic zone is provided first, and compared with our previous simulations (Oguz et al., 1997) in the absence of a dominant gelatinous carnivores group in the system. Next, the water column nitrogen structure is given with particular emphasis on the formation of the subsurface nitrate maximum and subsequent nitrate loss due to the denitrification taking place further below. Finally, the seasonal variations of the oxygen in the euphotic zone and the development of the suboxic layer are described with some remarks on the redox processes across the suboxic-anoxic interface region. A summary and conclusions are given in section 4.

2. Model Formulation

The annual variations of pelagic planktonic food web structure combined with the particulate matter decomposition and nitrogen cycling in the Black Sea interior waters are modeled here using the trophic interactions shown in Fig 2. We consider the nitrogen limited ecosystem involving two groups of phytoplankton (P_d, P_f) and of herbivorous/omnivorous zooplankton (Z_s, Z_l), a carnivorous macrozooplankton compartment Z_m, bacterioplankton B, labile pelagic detritus D, dissolved organic nitrogen DON, nitrate NO_3, nitrite NO_2, ammonium NH_4, dissolved oxygen O_2 and hydrogen sulphide H_2S. Two phytoplankton groups represent diatoms P_d and flagellates P_f, the latter including mainly dinoflagellates. The phytoplankton species differentiation is accompanied with the subdivision of herbivores into microzooplankton Z_s ($<200\ \mu m$) and mesozooplankton Z_l ($0.2 - 2mm$). The microzooplankton compartment consists of heterotrophic flagellates, ciliates, protoza and juvenile copepods, and is more efficient at consuming flagellates. The mesozooplankton compartment

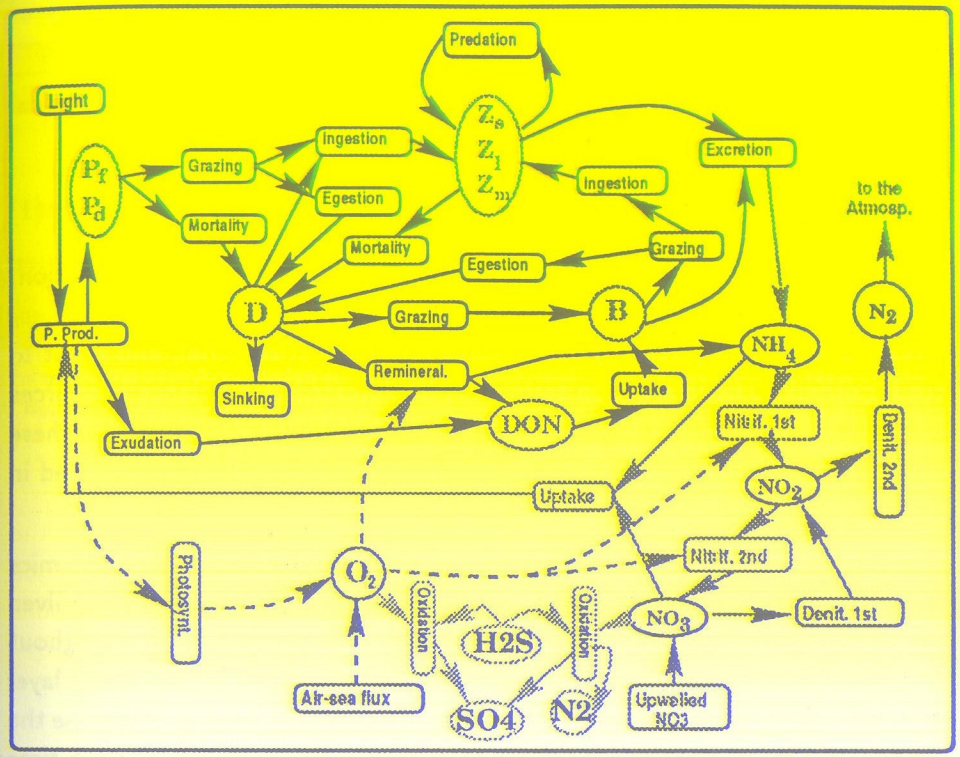

Figure 2: *A schematic diagram showing the biological processes and interactions included in the model*

is formed essentially by adult copepods fed primarily by diatoms and microzooplankton. The macrozooplankton compartment Z_m represents a particular gelatinous species group called the medusae "Aurelia aurita" which dominated the Black Sea ecosystem before the invasion of the ctenophore "Mnemiopsis leidyi" (Shushkina and Musayeva, 1990; Vinogradov and Shushkina, 1992).

The subdivision of the plankton compartments adopted here may not be entirely satisfactory to represent the diversity of all plankton groups within the central Black Sea. However, at this stage of the model development, it is difficult to introduce a more detailed representation, as their seasonal variations are generally not sufficiently documented and our knowledge of the biological vertical structure and fluxes is rather limited. Moreover, the absence of the gelatinous ctenophore "Mnemiopsis leidyi" as a separate macrozooplankton group in the model implies that our simulations are more appropriate for describing the central Black Sea ecosystem structure before the explosion of

the Mnemiopsis population during the late 1980's. Modeling the effect of Mnemiopsis on the Black Sea ecosystem is currently under investigation.

As in Oguz et al. (1996, 1997), the local temporal variations of all biological variables are expressed by equations of the general form

$$\frac{\partial F}{\partial t} + w_b \frac{\partial F}{\partial z} = \frac{\partial}{\partial z}\left[(K_b + \nu_b)\frac{\partial F}{\partial z}\right] + \Re_F \qquad (1)$$

where t is time, z is the vertical coordinate, ∂ denotes partial differentiation, K_b is the vertical turbulent diffusion coefficient, ν_b is its background value. w_b represents the sinking velocity for diatoms and detrital material, and is set to zero for others. The interaction term, $\Re_F$, is expressed as a balance of sources and sinks for each of the biological variables. A detailed description of these terms is provided below. The definition of parameters and their values used in the simulations are given in Tables 1 and 2.

The value of $K_b(z,t)$ is from the physical model of the mixed layer dynamics using the Mellor-Yamada level 2.5 turbulence closure parameterization. Given the daily, climatological wind stress and surface buoyancy forcing throughout the year, the model computes first the physical properties of the mixed layer structure (currents, temperature, salinity). They are then used to determine the intensity of the vertical mixing and the form of the eddy diffusivity at each time step. ν_b is parameterized according to Gargett (1984) in which the vertical eddy diffusivity associated with the internal wave activity is given by $\nu_b = aN^q$ where a is a constant with a typical value of $\sim 1\text{x}10^{-3} cm^2/s^2$, N is the square root of the Brunt-Vaisala frequency $[N \equiv -(g/\rho_0{}^{-1})(\partial\rho/\partial z)]^{1/2}$ and q is a constant varying between 0.5 and 1 whose value is estimated as 0.93 for the Black Sea by Samodurov et al. (1994). For the typical winter and summer stratifications generated by the model and taking $q = 1$, the upper limit estimate of ν_b attains almost uniform values of $\sim 7\text{x}10^{-6} m^2/s$ within the oxycline and suboxic layers throughout the year. Choosing $q = 0.5$ reduces this value by almost one order of magnitude. In the experiments, we take ν_b=$2\text{x}10^{-5} m^2/s$ within the upper 60m, decreasing linearly to $2\text{x}10^{-6} m^2/s$ at 75 m and then retaining this value within the rest of the water column. Thus, our choice of ν_b at subsurface levels of the model is regarded as an intermediate value derived from the Gargett formula, providing reasonably adequate representation of the vertical biochemical structure consistent with the observations.

The temperature provides an additional coupling between the physical and bio-

Table 1. Model parameters used in the numerical experiments

Parameter	Definition	Value
a	Photosynthesis efficiency parameter	0.01
k_w	Light extinction coefficient for PAR	0.08 m^{-1}
k_c	Phytoplankton self-shading coefficient	0.07 m^2 (mmol N)$^{-1}$
b_f, b_d, b_p, b_b	Food preferences of microzooplankton on flagellate, diatom, detritus, bacteria	0.7, 0.2, 1.0, 1.0
a_f, a_d, a_z, a_p, a_b	Food preferences of mesozooplankton on flagellate, diatom, microzoo, detritus, bacteria	0.2, 0.8,0.4,0.7,0.0
c_s, c_l	Food preferences of macrozooplankton on microzoo and mesozooplankton	0.0, 0.15
$\gamma_s, \gamma_l, \gamma_m$	Assimilation efficiencies	0.75, 0.75, 0.80
$\alpha_0, \alpha_1, \alpha_2, \alpha_3$	Oxygen to Nitrogen ratios	8.6, 8.6, 1.5, 0.5
α_4, α_5	Nitrogen to sulphide and Oxygen to sulphide ratios	4/3, 2.0
R_n	Half saturation constant in nitrate uptake	0.5 mmol N m^{-3}
R_a	Half saturation constant in ammonium uptake	0.2 mmol N m^{-3}
R_g	Half saturation constant for zooplankton grazing	0.5 mmol-N m^{-3}
R_d	Half saturation constant for detrital sinking	0.25 mmol-N m^{-3}
R_p	Half saturation constant for diatom sinking	0.5 mmol-N m^{-3}
R_b	Half saturation constant for bacterial uptake	0.5 mmol-N m^{-3}
R_o	Half saturation constant for oxygen limitation	10 mmol-O_2 m^{-3}
K_o	Constant for anaerobic oxygen limitation	2.5 mmol-O_2 m^{-3}
ψ	Ammonium inhibition parameter of nitrate uptake	3 (mmol N m^{-3})$^{-1}$
ϵ_n, ϵ_d	Detritus decomposition rates in aerobic and anaerobic conditions	0.1 day^{-1}
χ	Exudation rate	0.05
κ	Fraction of detritus remineralization directly converted to ammonium	0.8
$w_d{}^*$	Maximum detrital sinking rate	5.0 m day^{-1}
$w_p{}^*$	Maximum diatom sinking rate	1.0 m day^{-1}
Ω_a	Maximum ammonium oxidation rate	0.1 day^{-1}
Ω_n	Maximum nitrite oxidation rate	0.25 day^{-1}
Ω_d	Maximum nitrate reduction rate	0.015 day^{-1}
Ω_r	Maximum nitrite reduction rate	0.01 day^{-1}
Ω_o	Sulphide oxidation rate by oxygen	0.1 day^{-1}
Ω_s	Sulphide oxidation rate by nitrate	0.015 day^{-1}
Ω_m	Ammonium oxidation rate by nitrate	0.006 day^{-1}
ν_b	Background kinematic diffusivity for z$\leq$75m	$2\text{x}10^{-5} m^2 s^{-1}$
ν_b	Background kinematic diffusivity for z>75m	$0.2\text{x}10^{-5} m^2 s^{-1}$

Table 2. Model parameters used in the numerical experiments

Parameter	Definition	P_d	P_f	Z_s	Z_l	Z_m	B
Q_{10}	Q_{10} parameter in $f(T)$	1.2	1.2	2.0	2.0	2.2	2.5
σ_i and r_g	Growth and grazing rates	2.9	1.9	1.3	1.3	0.1-0.9	4.2
m_i and λ_i	Mortality rates	0.04	0.08	0.04	0.04	0.003-0.02	-
μ_i	Excretion rates	-	-	0.07	0.07	0.01	0.08

chemical models through a temperature dependent limitation functions of the plankton growth. The physical model, which has been documented previously in Oguz et al. (1996), is based on the one dimensional version of the Princeton Ocean Model implemented to the Black Sea by Oguz, Malanotte-Rizzoli and Aubrey (1995) and Oguz and Malanotte-Rizzoli (1996).

2.1. THE BIOLOGICAL SOURCE-SINK TERMS FOR THE PLANKTON EQUATIONS

Variations of the diatom and flagellate biomasses are governed by a balance between net primary production (the first terms on the right hand sides of eq's. 2,3) and losses due to zooplankton grazing (the second and third terms) and physiological mortality (the last terms). The effects of respiration and phytoplankton excretion are included in the latter loss terms. The phytoplankton growth is modeled for each group as the product of the maximum specific growth rate σ_i, the overall limitation function Φ and the phytoplankton concentration P_i. A fraction of the growth, represented by the parameter χ, is assumed to be exuded as the dissolved organic material (DON). The maximum growth is limited by a factor defined by the minimum of the light and nutrient limitation terms, $\alpha(I)$ and $\beta_t(NO_3, NH_4)$ respectively, multiplied with the temperature limitation function $f_p(T)$. $\beta_t(NO_3, NH_4)$ is given as the sum of nitrate limitation function $\beta_n(NO_3)$ and the ammonium limitation function

$\beta_a(NH_4)$. The nitrogen is considered as the only limiting nutrient for the phytoplankton growth in the central Black Sea. The silicate limitation on the diatom growth is not therefore taken into account. The temperature limitation function is expressed by

$$f_p(T) = Q_{10p}^{(T-20)/10} \tag{8}$$

Flagellates	P_f	$\Re_{Pf} = (1-\chi)\,\sigma_f \Phi P_f - G_s(P_f)\,Z_s - G_l(P_f)\,Z_l - m_f P_f$	(2)
Diatoms	P_d	$\Re_{Pd} = (1-\chi)\,\sigma_d \Phi P_d - G_s(P_d)\,Z_s - G_l(P_d)\,Z_l - m_d P_d$	(3)
Microzoo	Z_s	$\Re_{Zs} = \gamma_s [G_s(P_f) + G_s(P_d) + G_s(D) + G_s(B)]\,Z_s - G_l(Z_s)\,Z_l - G_m(Z_s)\,Z_m - \mu_s Z_s - \lambda_s Z_s^2$	(4)
Mesozoo	Z_l	$\Re_{Zl} = \gamma_l [G_l(P_f) + G_l(P_d) + G_l(D) + G_l(Z_s)]\,Z_l - G_m(Z_l)\,Z_m - \mu_l Z_l - \lambda_l Z_l^2$	(5)
Macrozoo	Z_m	$\Re_{Zm} = \gamma_m [G_m(Z_s) + G_m(Z_l)]\,Z_m - \mu_m Z_m - \lambda_m Z_m$	(6)
Bacteria	B	$\Re_B = G_b(DON)\,B + G_b(D)\,B - G_s(B)\,Z_s - G_l(B)\,Z_l - \mu_s B$	(7)

Changes in the zooplankton biomasses are controlled by ingestion, predation, mortality and excretion. Ingestion is represented in eq'.s (4)-(6) by the terms inside the square brackets multiplied with $\gamma_i's$. The subsequent two terms in eq. (4) represent microzooplankton predation by others. A similar predation term also follows the ingestion term in eq. (5). The last two terms of eq's (4)-(6) define excretions and mortalities, respectively. We note that the microzoo and mesozooplankton mortalities are expressed in the quadratic form. The grazing terms, $G_i(\psi_j)'s$, are expressed by Michaelis-Menten relation using the food capture efficiencies shown in Fig. 3 (see Oguz et al., 1997 for the details). The maximum specific grazing rates (rations) used in these expressions are controlled by the temperature according to eq. (8).

In eq. (5), the maximum grazing rate and the mortality rate of the medusae population are varied seasonally in order to model their life cycle in a simplest possible way. According to the available observations (Shushkina and

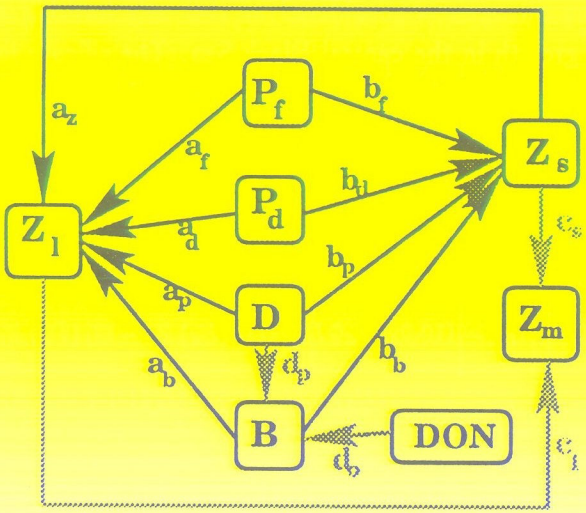

Figure 3: *Trophic interactions between different plankton groups and related food preference coefficients used in the model*

Musayeva, 1983; Lebedeva and Shushkina, 1991; Olesen et al., 1994), the are two particular periods of increased medusae production as spring and autumn. Lateral transport of juveniles from coastal regions also accounts for an important source of their biomass increase in the central Black Sea during this period. These two effects are parameterized in the model by an exponential increase of the maximum ration from its background value of 0.1 to 0.9 day^{-1} within a week at the beginning of April. The maximum ration is kept at this value until the last week of May, and then decreased exponentially again to its background value. The second biomass increase occurs in October. A similar exponential increase on the maximum ration is thus specified during the second week of September. The June-July period and the winter season are, on the other hand, characterized by the lowest level of their stock because of major death events. This process is parameterized by an order of magnitude increase of the mortality rate from 0.002 to 0.03 day^{-1} during these particular periods.

Modeling the temporal and vertical distributions of bacterioplankton is one of the most challenging aspects of the Black Sea biogeochemistry, since different bacterial populations play different roles in different parts of the water column from the surface to the suboxic/anoxic interface zone. In the present study, we simply consider only one aggregated bacterial group; the dissolved and particulate organic materials constitute primary sources for their growth. We therefore ignore the ammonium uptake of bacterioplankton, and assume that their nitrogen requirements are met by the DON uptake only (Walsh and Dieterle, 1994). The grazing of bacterioplankton by micro- and mesozooplankton, their excretion in the form of ammonium represent the sink terms. The effect of bacterial mortality is included in the excretion term.

2.2. THE SOURCE-SINK TERMS FOR THE EQUATIONS OF PARTICULATE AND DISSOLVED FORMS OF ORGANIC MATERIAL

Particulate Org. Matter	D	$\Re_D = (1-\gamma_s)\left[G_s(P_f)+G_s(P_d)+G_s(B)\right]Z_s+$ $(1-\gamma_l)\left[G_l(P_f)+G_l(P_d)+G_l(Z_s)\right]Z_l$ $+(1-\gamma_m)\left[G_m(Z_s)+G_m(Z_l)\right]Z_m$ $+\left[m_s P_s + m_l P_l + \lambda_s {Z_s}^2 + \lambda_l {Z_l}^2 + \lambda_m Z_m\right]$ $-\gamma_s G_s(D)\,Z_s - \gamma_l G_l(D)\,Z_l - G_b(D)\,B$ $-\left[\epsilon_n f_n(O_2)+\epsilon_d f_d(O_2)\right]D$	(9)
Dissolved Org. Matter	DON	$\Re_{DON} = -G_b(DON)\,B + \chi\left[\sigma_f \Phi P_f + \sigma_d \Phi P_d\right]$ $+(1-\kappa)\left[\epsilon_n f_n(O_2)+\epsilon_d f_d(O_2)\right]D$	(10)

Fecal pallets, constituting the unassimilated part of ingested food (the group of terms inside the first three square brackets in eq. 9), as well as dead phytoplankton and zooplankton (the terms inside the fourth square bracket) are the sources of labile particulate organic matter (detritus). They are recycled in the water column as a result of ingestion by zooplankton and bacteria (represented by the terms involving $G_s(D)$, $G_l(D)$, $G_b(D)$) and decomposition into the dissolved organic nitrogen form in the aerobic and anaerobic parts of the water column (terms inside the last square bracket). For DON, the phytoplankton exudation and detritus breakdown form the sources whereas the bacterial uptake contitutes the loss. A certain fraction of the total particulate material is converted to DON to be utilized eventually for bacterial growth. The rest is transported directly to the ammonium form.

The particulate organic material is considered to sink with a single settling

velocity w_d, which varies according to detritus concentration as

$$w_d(z) = w_d^* \left[\frac{D}{R_d + D} \right] \tag{11}$$

where w_d^* represents the maximum sinking velocity and R_d is the half saturation constant. A similar formalism is also adopted for parameterizing sinking of diatoms. This formulation simply specifies higher sinking speeds of diatoms and particulate materials when they are aggregated at higher concentrations.

The efficiency of aerobic decomposition, which occurs at the rate $\epsilon_n f_n(O_2) D$ in the oxygenated part of the water column, is considered to decrease by decreasing oxygen concentrations, and to terminate at oxygen concentrations less than 3 μM. This choice of treshold value is consistent with the observations (e.g. Lipschultz et al., 1990) which report a range of values between 1 and 5 μM in different oceanic regions. The oxygen limitation function $f_n(O_2)$ controlling this process is expressed by

$$f_n(O_2) = \frac{O_2}{O_2 + R_O} \qquad for \qquad O_2 \geq 3\mu M \tag{12}$$

with R_O denoting the half saturation constant.

When oxygen is depleted in the water column, decomposition of particulate material occurs anaerobically by utilizing the nitrate, abundant below the euphotic zone. This process is controlled by the oxygen concentrations according to

$$f_d(O_2) = \left[\frac{K_O}{K_O + O_2} \right] \quad for \quad O_2 < 3\mu M \tag{13}$$

It implies a maximum rate of anaerobic decomposition at zero oxygen concentration and a gradual decrease as the oxygen concentration increases. When $O_2 \geq 3\mu M$, $f_d(O_2)$ is set to zero.

2.3. THE SOURCE-SINK TERMS FOR THE NITROGEN, O_2 AND H_2S EQUATIONS

In eq. 14, excretions by three zooplankton groups and bacteria (the terms inside the first square brackets) as well as the part of the particulate matter remineralized without taking part in the bacterial growth (the terms in the last square brackets) constitute the ammonium sources. An ammonium flux is imposed at the lower boundary of the model (see eq. 24) to incorporate

response of the ammonium pool in the anoxic layer of the Black Sea. The losses are its uptake during phytoplankton production (the second term) and oxidation to the nitrite form in the aerobic conditions (the third term) as the first step of the nitrification process. In the anaerobic conditions, the ammonium is considered to be oxidized by nitrate available within the lower part of the SOL. This process is crucially important for depletion of NH_4 within the SOL, as suggested by the available observations. Otherwise, in the absence of any ammonium oxidation, it keeps diffusing upwards continuously from its pool within the anoxic layer, and should builds up gradually within the SOL in time.

Ammonium	NH_4	$\Re_{NH4} = [\mu_s Z_s + \mu_l Z_l + \mu_m Z_m + \mu_b B] - \Phi\left(\frac{\beta_a}{\beta_t}\right)(\sigma_s P_s + \sigma_l P_l) - \Omega_a f_n(O_2) NH_4 + \kappa[\epsilon_n f_n(O_2) + \epsilon_d f_d(O_2)] D$	(14)
Nitrite	NO_2	$\Re_{NO2} = \Omega_a f_n(O_2) NH_4 - \Omega_n f_n(O_2) NO_2 + \Omega_d f_d(O_2) NO_3 - \Omega_r f_d(O_2) NO_2$	(15)
Nitrate	NO_3	$\Re_{NO3} = \Omega_n f_n(O_2) NO_2 - \Omega_d f_d(O_2) NO_3 - \Phi\left(\frac{\beta_n}{\beta_t}\right)(\sigma_s P_s + \sigma_l P_l) - \alpha_4 \Omega_s H_2S$	(16)
Oxygen	O_2	$\Re_{O2} = \alpha_0(\sigma_s \Phi P_s + \sigma_l \Phi P_l) - \alpha_1 \epsilon f_n(O_2) D - \alpha_2 \Omega_a f_n(O_2) NH_4 - \alpha_3 \Omega_n f_n(O_2) NO_2 - \alpha_5 \Omega_o H_2S$	(17)
Hydrogen Sulphide	H_2S	$\Re_{H2S} = -\Omega_s H_2S - \Omega_o H_2S$	(18)

The data (Codispodi et al., 1991; Basturk et al., 1994) indicate that nitrite concentrations in the euphotic zone are always smaller than the other forms of nitrogen. Thus, the contribution of nitrite uptake to the phytoplankton production is expected to be small. This was further confirmed by Oguz et al. (1997). Then, the nitrite equation involves only the oxidation-reduction reactions associated with the nitrification and denitrification processes. In eq. 15, the first two terms represent the ammonium to nitrite and nitrite to nitrate

oxidation reactions of the nitrification process in the oxygenated waters. The third and fourth terms, on the other hand, represent the denitrification process in the oxygen deficient conditions with the third term modeling the nitrate to nitrite reduction and the fourth term representing the nitrite reduction to the form of nitrogen gas (the second stage of the denitrification). Since the nitrogen gas eventually escapes to the atmosphere, this term implies a net nitrogen loss from the system.

The nitrate equation (16) consists of a source term due to the nitrification (the first term). The loss terms are associated with its uptake by the phytoplankton production (the third term), the nitrate reduction (the second term), and its consumption in the H_2S oxidation processes (the fourth term). α_4 gives the stoicheiometric coefficient for the nitrate to hydrogen sulfide ratio.

The source/sink terms of the oxygen equation (17) are the photosynthetic production in the euphotic zone, consumption during the bacterial decomposition of organic material, ammonium and nitrite oxidations in the nitrification process, as well as during the H_2S oxidation. The ocean-atmosphere exchange is introduced as a boundary condition (see Section 2.3). $\alpha_0, \alpha_1, \alpha_2, \alpha_3$ are the stoicheiometric coefficients of the oxygen to nitrogen ratio and α_5 is the oxygen to hydrogen sulphide ratio.

Eq. (18) describes the hydrogen sulphide oxidation using the oxygen and nitrate present in the suboxic zone. H_2S is supplied to this layer from the anoxic pool by the prescribed flux at the bottom boundary of the model (eq. 21). After transported upward through the anoxic layer, it first interacts with the nitrate at the oxygen-depleted lower part of the SOL. In the case that H_2S is transported further upwards within the SOL, the available oxygen resource is also utilized for its oxidation. In the model this reaction is considered to occur at $O_2 > 0.5\mu M$. The end product of these reactions is the SO_4 formation as well as export of nitrogen gas (N_2) to the atmosphere. We recall that H_2S generation by the sulfur reduction process as well as other redox processes which are thought to regulate the suboxic layer dynamics (see Murray et al., 1995) are not incorporated in this model.

2.4. BOUNDARY CONDITIONS

The bottom boundary of the model, h_b, is taken at the depth of 150 m. This roughly corresponds to the base of the permanent pycnocline zone at the 16.4 kg/m^3 density level, and is situated at least 25 m below the base of the suboxic layer. Its location therefore is chosen to be reasonably away from the domain of interest in this model study. Except otherwise specified, all the turbulent fluxes are set to zero at the surface and bottom boundaries for all the state variables. In the diatom and detritus equations, this condition is extended to include absence of the particulate matter and diatom fluxes at the boundaries. In the most general form, we then specify the bottom and surface boundary conditions as

$$\left[(K_b + \nu_b)\frac{\partial F}{\partial z}\right] + w_b F = 0 \qquad at \;\; z = 0 \;\; and \;\; z = -h_b \tag{14}$$

A justification for the assumption of no export flux of particulate matter from the bottom boundary was given by Oguz et al. (1996, 1997).

In the oxygen equation, the air-sea exchange process is expressed in terms of the "stagnant film" model of Broecker and Peng (1982) as

$$\left[(K_b + \nu_b)\frac{\partial O_2}{\partial z}\right]_{z=0} = V_p\left[{O_2}^{sat} - O_2\,(z=0)\right] \tag{15}$$

where V_p is the piston velocity taken as 3 m/day in the simulation experiments. ${O_2}^{sat}$ represents the oxygen saturation concentration computed according to UNESCO (1986) formula using the surface temperature and salinity values of the physical model at each time step.

The H_2S and NH_4 fluxes are prescribed at the bottom boundary as

$$\left[(K_b + \nu_b)\frac{\partial \varphi}{\partial z}\right] = FLX(\varphi) \qquad at \;\; z = -h_b \tag{16}$$

where $FLX(\varphi)$ represents the hydrogen sulphide and ammonium fluxes at the bottom boundary. Their values are adjusted to reproduce their observed concentrations near the anoxic boundary.

2.5. INITIAL CONDITIONS AND NUMERICAL PROCEDURE

The physical model is initialized by a stably stratified upper ocean temperature and salinity profiles representative of the autumn conditions for the interior part of the sea. It is forced by the monthly climatological wind stress and surface thermal fluxes (see Table 2 in Oguz et al., 1996) whereas no-stress, no-heat and no-salt flux conditions are specified at the bottom. The biochemical model

is initialized by a vertically uniform nitrate and ammonium concentration of 3.5 mmol/m^3 and 0.5 mmol/m^3, respectively, throughout the water column. The oxygen is initially set to 50 μM within the upper 55 m, 15 μM down to 115 m and zero further below near the lower boundary of the model. Other state variables of the biochemical model are initialized with small constant values over the water column. The model therefore specifies rather arbitrary initial conditions and does not possess any given a priori vertical biochemical structure. Our simulations are therefore independent from the initial conditions.

The set of equations given in the previous section yields

$$\frac{\partial \sum F}{\partial t} = \frac{\partial}{\partial z}\left[(K_b + \nu_b)\frac{\partial \sum F}{\partial z} + w_b \sum F\right] \qquad (17)$$

where summation is taken over all the prognostic variables contributing to the nitrogen balance of the system. In the light of eq. 22, this expression thus implies that the total initially prescribed nitrogen content (i.e the sum of the initial nitrate and ammonium concentrations within the water column) is conserved throughout the integration period. The model will simply utilize the initial nitrogen stock to generate living and nonliving components of the biological system. The oxygen, on the other hand, has a continuous interaction with the atmosphere. Its final state will therefore be governed by the external conditions as well as the biological processes taking place within the water column.

The choice of different vertically uniform initial nitrate concentrations does not affect the form of the final equilibrium structure of NO_3. Its value prescribed here is based on the vertical integration of a typical nitrate profile representative of the central Black Sea conditions. Smaller values simply result in lower nitrate peaks, as well as weaker phytoplankton blooms. The choice of the initial ammonium concentration is also not critical to the model evolution. Within the oxygenated part of the water column, the initial ammonium acts as a part of the nitrogen uptake in the autumn phytoplankton production. Near the lower boundary, the bottom flux governs its vertical structure immediately after starting the time integration.

The details of the numerical solution procedure are described in Oguz et al. (1996). A total of 50 vertical levels is used to resolve the 150 m thick water column. A time step of 5 minutes is used in the numerical integration of the system of equations. First, the physical model is integrated for five years to

achieve a yearly cycle of the upper layer physical structure. Using these results, the biochemical model is then integrated for four years which is sufficient to complete its transient adjustment period from the initial conditions.

2.6. TRANSIENT ADJUSTMENT

The vertically uniform initial nitrate structure adjusts itself to changes in the system near the surface and bottom boundaries of the model within a few months after the begining of the time integration. The entrainment associated with the winter cooling tends to build up a uniform nitrate structure within the convectively generated winter mixed layer, whereas the nitrogen cycling leads to accumulation of nitrate below the seasonal thermocline during the following summer. Near the bottom of the model, the denitrification process expressed by the second term in eq. 16 erodes gradually the initial nitrate structure and forms a lower nitracline zone within the first year of integration.

In the oxygenated waters, the initial oxygen concentration of 50 μM is taken purposedly to be much smaller than the typical observed values (around 300 μM). In fact, our choice of this value is unimportant since external sources (i.e. the air-sea flux) governing the oxygen dynamics develop a typical observed structure shortly after the start of the model integration.

In the deeper parts of the water column where the suboxic zone is expected to form, the initial oxygen concentration specified is higher than the one typically available at these levels. Once the biological pump starts functioning, the initial oxygen concentration at these levels decrease gradually (due to remineralization and nitrification) until it reaches its trace level values in the suboxic zone. The transient adjustment is completed to a large extent within the first year and the system approaches to an equilibrium state within the following two years. Specification of higher initial oxygen values only prolongs the transient adjustment time, but does not alter the vertical oxygen structure of the final state.

3. Model Results

Results from the simulation experiments performed using the parameter set given in Tables 1 and 2 are described here. The input parameters are obtained from the available observations in the Black Sea as well as from other similar

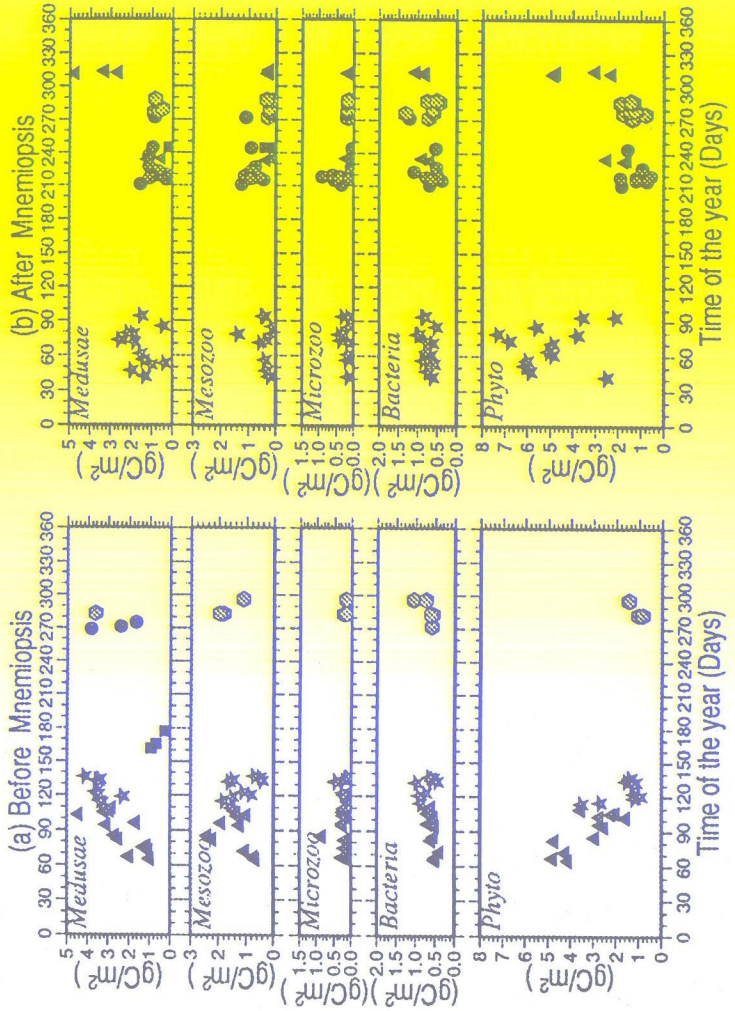

Figure 4:

ecosystems such as the Baltic and the North Seas. Using a series of sensitivity experiments, the parameters are optimized to provide reasonably realistic simulations. The reader should refer to Oguz et al. (1996, 1997) for more details on the specifications of the input parameters, and their sensitivity on the pelagic food web structure.

We compare our model results on the phyto-, zoo- and bacterioplankton communities with the data collected within the central Black Sea by the Shirshov Institute of Oceanology-Moscow since 1978 (Shuskina et al., 1997). The data is summarized in Fig. 4 in two different periods designated as "before" and "after" the Mnemiopsis that invaded the Black Sea during late 1980's. Its population exploded during 1987-1988, and caused major changes in the ecosystem since they almost depleted forage mesozooplankton, fish egg and larvae stocks whereas they are a dead end of the food chain. Our model, at this stage, does not incorporate the Mnemiopsis as a separate zooplankton compartment. Our results therefore are more appropriately compared with the data given for the "before the Mnemiopsis" period in Fig. 4a. But, the data for the period "after the Mnemiopsis" are also included here as supplementary information (Fig. 4b).

The comparison of the model results on the water column nitrogen, dissolved oxygen and H_2S structures are based on the data obtained by the R.V. Knorr cruise and a series of field surveys performed in 1990's by the R.V. Bilim of the Institute of Marine Sciences of the Middle East Technical University in Turkey.

3.1. WATER COLUMN PLANKTON STRUCTURE

The phytoplankton structure simulated by the model is shown in Fig. 5a as the yearly distribution of the euphotic zone integrated biomasses. Diatoms are responsible for generating the strongest phytoplankton bloom of the year which starts at the end of February, and lasts until the end of March. The peak biomass value is around 50 mmol N/m^2 which, in terms of the carbon units (assuming carbon to nitrogen ratio of 8.5 for the Black Sea in general), is equivalent to approximately 5 gC/m^2. This value is in good agreement with the observed values; particularly with those obtained during 1980's (Fig. 4a). More recent measurements performed during late 1980's and early 1990's (Fig. 4b) however suggest somewhat higher values up to about 7 gC/m^2 because of the weakening of the mesozooplankton grazing pressure after the "invader"

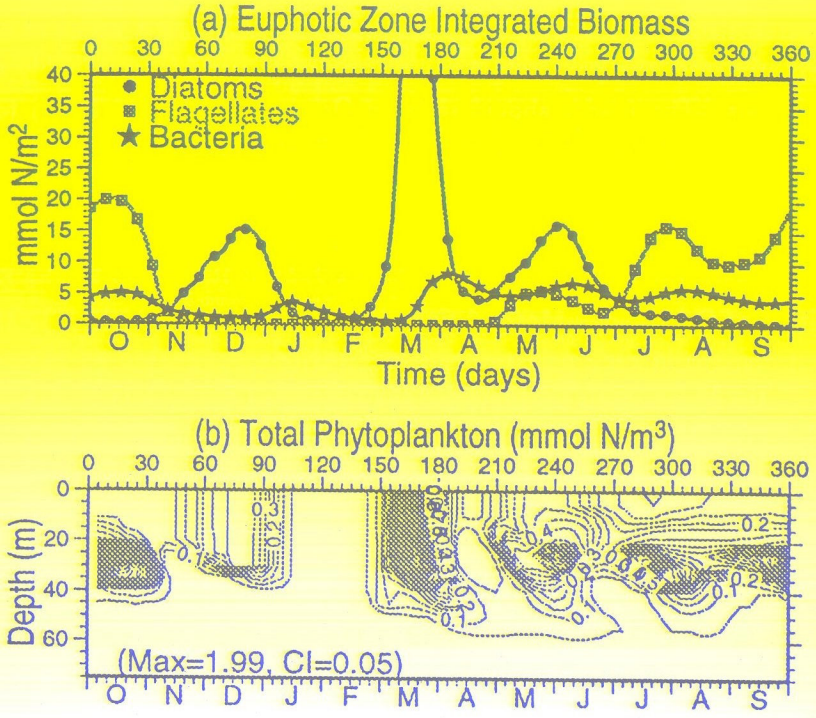

Figure 5: *Annual distribution of the (a) euphotic zone integrated phytoplankton and bacterioplankton biomasses, (b) vertical structure of the total phytoplankton biomass within the upper layer water column*

ctenophore Mnemiopsis. The diatoms exhibit an appreciable structure during the rest of the year too. Two pronounced increases of their biomass up to $\sim$ 15 mmol N/m^2 occur in late spring (from mid-May to mid-June) and in December. It may be inferred from the vertical structure of the total phytoplankton distribution (Fig. 5b) that the March and December blooms are surface-intensified events. They extend to the depth of 40-50 m coinciding approximately with the depths of winter convective overturning and the 1 % light level. Their formation is the result of entrainment of subsurface nitrates by the convective overturning and therefore is related to the new production. The late spring diatom bloom, on the other hand, is a subsurface event between the seasonal thermocline and the base of the euphotic zone and is essentially originated by the regenerated production.

Contrary to the diatoms, the flagellate group is more active during the summer. After a slight increase in their biomass ($\sim$ 5 mmol N/m^2) at the time of late spring diatom production, the major flagellate bloom takes place from mid-July to mid-August in comparable magnitude with the previous diatom bloom. The enhanced flagellate production persists effectively till the end of October with some variations in its biomass; e.g. decreasing to $\sim$ 10 mmol N/m^2 level by the end of September and increasing to $\sim$ 20 mmol N/m^2 by mid-October. It is noted from Fig. 5b that these are sub-thermocline productions, and as we shall see in the next section, they are caused by efficient nitrogen recycling at these depths. No flagellate however remains after October till the next spring. Unfortunately, the phytoplankton data shown in Fig. 4a do not have a good coverage for the summer and autumn seasons. But, the July and October flagellate blooms as well as the December diatom bloom are supported by the data given in Fig. 4b, even though the observed autumn bloom is stronger and occurs slightly earlier, in mid-November. Furthermore, the chlorophyll-a data presented in Oguz et al. (1997) and Vedernikov and Demidov (1997) also suggest a reasonably good representation of the annual phytoplankton distribution in the central Black Sea by the model.

As compared to diatoms and flagellates, bacterioplankton biomass exhibits a somewhat weaker distribution within the euphotic zone throughout the year (Fig. 5a). The stock is typically less than $\sim$0.5 gC/m^2 in the late autumn and winter months. It almost doubles itself after the March diatom bloom till the end of summer. The majority of the summer bacterioplankton population is located below the seasonal thermocline at the same levels with the flagellates. The simulated annual bacterioplankton distribution seems to be consistent with the data (Fig.'s 4a,b) which reveal slightly higher biomasses after the Mnemiopsis invasion. This is, however, expected since increasing the biomass of gelatinous species should ultimately cause an increase on the particulate and dissolved organic matter contents. This in turn should lead to some increase in the bacterioplankton population in the system.

A major increase in the mesozooplankton stock takes place following the diatom bloom (Fig. 6a). As the grazing pressure introduced by the mesozooplankton decreases the diatom population towards the end of March, mesozooplankton biomass keeps increasing in the euphotic zone. The maximum biomass of about 4 gC/m^2 is comparable with the diatom population, whereas

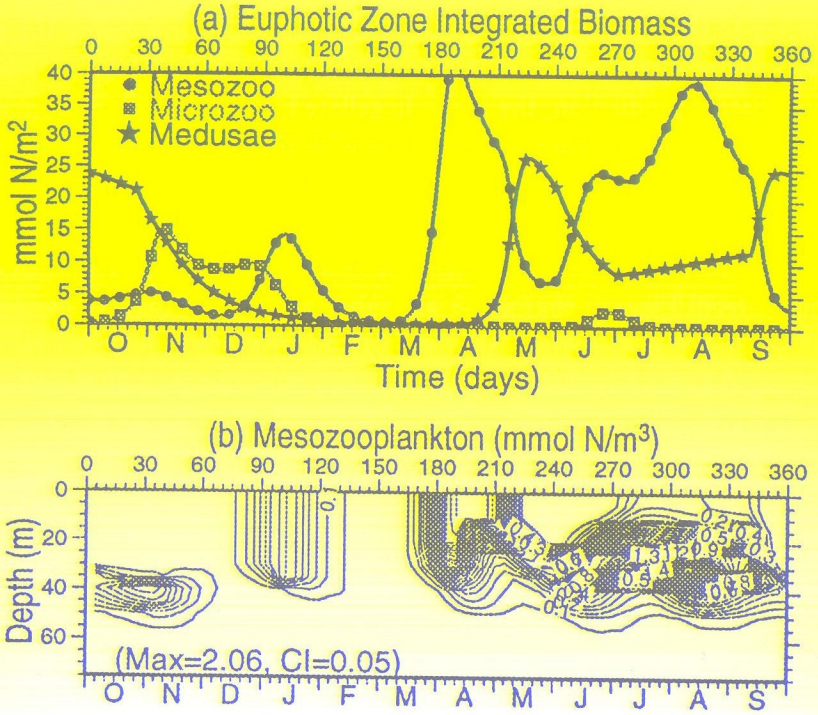

Figure 6: *Annual distribution of the (a) euphotic zone integrated zooplankton biomasses, (b) vertical structure of the mesozooplankton biomass within the upper layer water column*

slightly lower values around 2.5 gC/m^2 are suggested by the data (Fig. 4a). The mesozooplankton biomass decreases in May and rises later in the summer with a maximum value of ~4 gC/m^2 in August right after the first flagellate bloom. A major decline in the biomass to a value of ~0.5 gC/m^2 takes place in September. A secondary increase on the mesozooplankton stock up to ~1.5 gC/m^2 follows the December diatom bloom event. The winter (January) and late March mesozooplankton growths take place in the upper 40 m water column, whereas the summer growth is confined below the seasonal thermocline consistently with the annual phytoplankton production sequence (Fig. 6b).

The microzooplankton biomass remains negligibly small throughout the year (Fig. 6a), because of its almost complete predation by the mesozooplankton community. The observations (Fig. 4a,b) tend to indicate a microzooplankton biomass of about 0.5 gC/m2. Slight adjustment on the food preference coefficients might in fact provide a better estimate of the microzooplankton biomass.

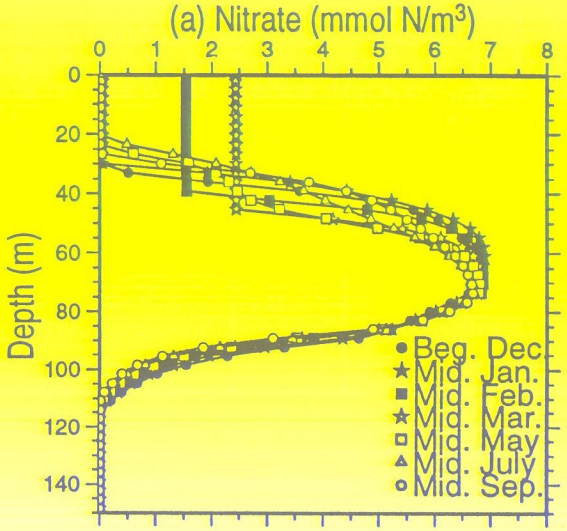

Figure 7: *(a) The model simulated daily averaged nitrate profiles versus depth at selected times of the year*

The Medusae biomass exhibits two major peaks during the year (Fig. 6a). The first one follows the mesozooplankton development in spring. The biomass reaches a maximum value of ~2.8 gC/m^2 in May as they deplete the mesozooplankton stock available for their growth. The summer season is identified by a general decrease in their population to a minimum level of ~1.0 gC/m^2. In agreement with the externally specified time dependent maximum growth rate in the model, the second increase in the medusae population takes place at the begining of October following the abundance of mesozooplankton stock in the system. The population decays during the winter months, until a new cycle of growth and reproduction begins in April. Following the vertical structure of the mesozooplankton community, the first medusae growth event is distributed uniformly within the upper 40 m, whereas the second event is confined below the seasonal thermocline. The data (Fig. 4b) suggest values varying from 2 to 4 gC/m^2 during the peak medusae growth periods, and minimum values less than 1 gC/m^2 during summer. The model estimates thus lie within the range

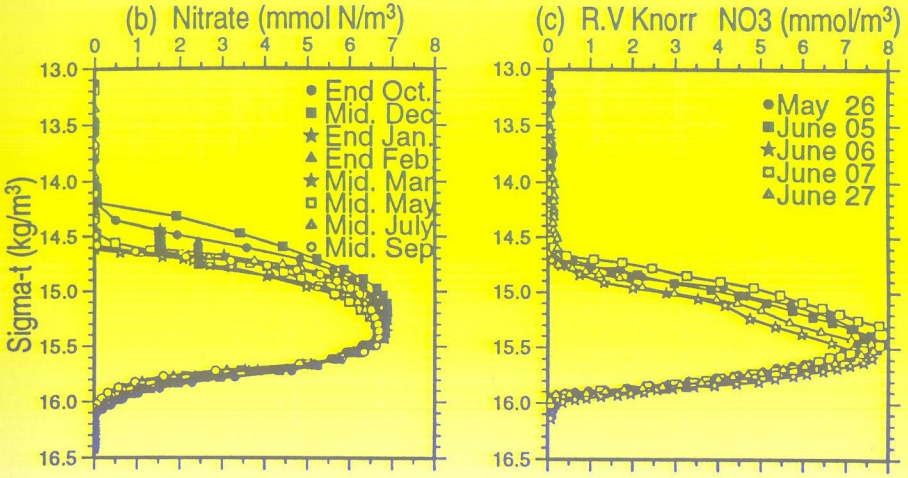

Figure 7: *(b) The model simulated daily averaged nitrate profiles versus density at selected times of the year, (c) the observed nitrate profiles versus density obtained by the R.V Knorr surveys in the Black Sea during summer 1988.*

of variability of the measured values. The form of the annual medusae distribution predicted by the model agrees reasonably well with the data presented in Fig. 4, as well as with the findings reported by Lebedeva and Shushkina (1991).

We note from Fig's 5a and 6a that the peaks of the phytoplankton (diatoms and flagellates) and the zooplankton (mesozoo and macrozoo) biomasses march sequentially one after the other as a result of their prey-predator interactions. As soon as the diatom bloom degrades, the mesozooplankton biomass starts increasing as they assimilate the diatoms. Their biomass tends to decline during May, which coincides with the period of Medusae growth. At the same time, as the grazing pressure put by mesozooplankton is relaxed, the diatoms and partly the flagellates have the possibility of growing with peaks towards the end of May. The summer mesozooplankton growth is principally caused by the decline of medusae population, with additional contributions by the degradation of the phytoplankton blooms towards the end of June. A similar interaction between mesozooplankton and medusae taking place earlier in May repeates itself once again during September.

3.2. WATER COLUMN NITROGEN STRUCTURE

A series of nitrate profiles plotted versus depth and sigma-t at selected times of the year is shown in Fig. 7a,b respectively. Prior to the March diatom bloom event, the nitrate concentrations attain values in excess of 2 mmol/m^3 within the upper 50 m water column during the winter months (Fig. 7a). The summer mixed layer concentrations, on the other hand, do not exceed 0.2 mmol/m^3 because of the lack of sufficient supply from the subsurface levels across the strong seasonal thermocline/pycnocline. In the region below the seasonal thermocline, a linear increase of the nitrate concentrations takes place up to 6 mmol/m^3 at 50 m depth. The nitrate accumulated in this region supports the summer subsurface phytoplankton production shown in Fig. 5b. Further below, the nitrate profiles possess a distinct maximum of about 7 mmol/m^3 near 70 m. The peak is broader and stronger during the autumn and winter corresponding to a more active nitrogen recycling phase after the spring and summer phytoplankton productions.

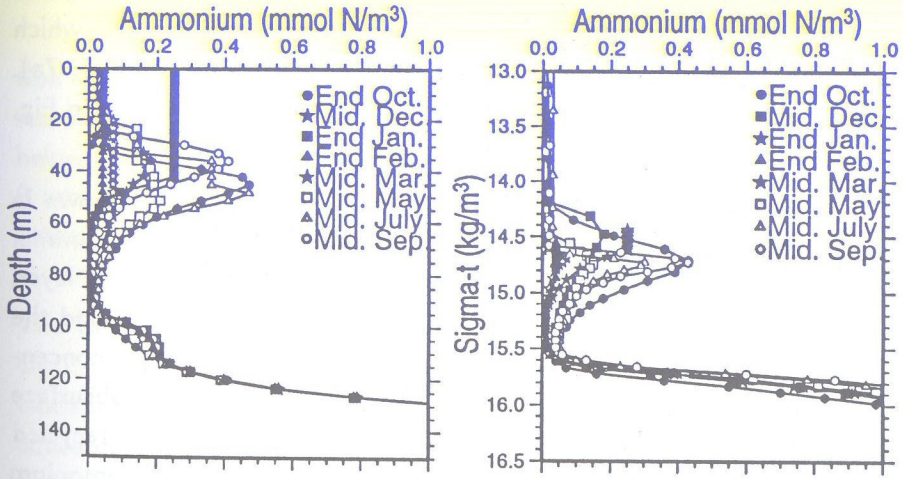

Figure 8: *(a) The model simulated daily averaged ammonium profiles versus depth (left) and versus density (right) at selected times of the year*

Considering the fact that the upper layer water column of the Black Sea has a very strong density stratification, and that the properties are distributed almost uniformly along the isopycnal surfaces, it is customary to express vertical variations of the biochemical properties in the Black Sea using the density as

the vertical coordinate. When the nitrate profiles are plotted against density (Fig. 7b), the position of the peak coincides approximately with the 15.4 sigma-t level. This is supported by the observations (Tugrul et al., 1992; Basturk et al., 1994; Murray et al., 1996; and others), even though the six repeated casts at 42 50 N and 32 00 E during the period of 26 May-27 June 1988 in the R.V Knorr surveys suggest some degree of variability of the peak position between 15.3 and 15.6 sigma-t levels (Fig. 7c). Furthermore, this particular data set provides maximum nitrate values of about 8.0 mmol/m^3 which are about 1 mmol/m^3 higher than our simulations. However, the other data sets indicate regional as well as year to year variability of the nitrate maximum. They tend to suggest that the peak concentrations vary in the range from 6 to 8 mmol/m^3.

It will be shown in the following section that the position of the nitrate maximum is intimately related with the location of the onset of trace level oxygen concentrations as they control the lower limit of the nitrification and the onset of the denitrification in the water column. The computed nitrate profiles do not possess any seasonal variability below the peak. They tend to decrease uniformly to their trace level values around 16.0 sigma-t level (Fig. 7b), which is located roughly 40 m below the position of the nitrate maximum (Fig. 7a). An almost similar trend also can be seen in the observed profiles given in Fig. 7c.

The corresponding ammonium profiles computed by the model are shown in Fig. 8a. As suggested by the observations (Codispoti et al., 1991), the summer period is characterized by depleted ammonium stocks within the mixed layer, followed by peak concentrations of the order of 0.2-0.4 mmol/m^3 around the base of the euphotic zone. These elevated sub-thermocline ammonium concentrations are a consequence of active nitrogen recycling following the subsurface summer plankton production. During the less productive and poorly-recycled winter months, these peaks are eroded to a large extent as the ammonium is oxidized to the nitrate form, except in the recycling phase right after the December diatom bloom as depicted in Fig. 8a by the January profile. The consistency of the model simulated summer ammonium peaks (in terms of their vertical positions and intensities) with the observations were shown previously by Oguz et al. (1997).

At deeper levels, all the ammonium profiles exhibit consistently minimum concentrations below 70 m depth and 15.4 kg/m^3 sigma-t level which is the location corresponding to the nitrate maximum (Fig. 7b). The concentrations are less than 0.2 mmolN/m^3 within the suboxic zone. They increase rather sharply below the 16.0 kg/m^3 sigma-t level, reaching at the values of 1 mmol/m^3 and 9 mmol/m^3 near the 16.25 and 16.45 sigma-t levels, respectively. Such ammonium variations within the anoxic layer are supported by the observations shown in Fig. 8b.

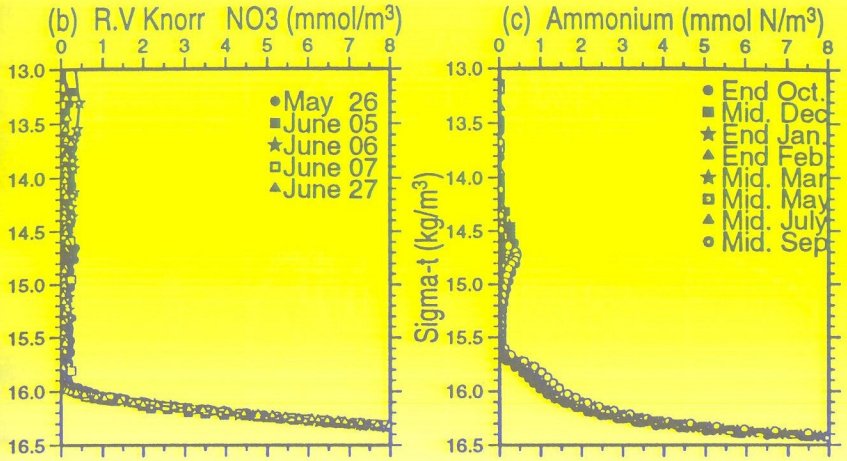

Figure 8: *(b) the observed ammonium profiles versus density obtained by the R.V Knorr surveys in the Black Sea during summer 1988, (c) The model simulated daily averaged nitrate profiles versus density at selected times of the year in the absence of the ammonium oxidation in anaerobic conditions.*

The importance of the NH_4 oxidation in unaerobic conditions (i.e. when $O_2 < 3\mu M$) is demonstrated in Fig. 8c. In the absence of the ammonium oxidation within the anoxic water (i.e. Ω_m=0), the profiles reveal much higher concentrations within the suboxic layer. Starting from approximately 15.6 kg/m^3 sigma-t level at 85 m depth, the euphotic zone ammonium structure is connected to the deep ammonium pool by concentrations of 1 mmol/m^3 $\sigma_t \sim$ 15.9 kg/m^3 and 3 mmol/m^3 at $\sigma_t \sim$ 16.25 kg/m^3. The elevated ammonium concentrations in the suboxic layer are formed as a result of the continuous upward diffusive transport from the bottom source during the several years of model integration.

The vertical nitrite structure exhibits two distinct peaks (Fig. 9a). The first

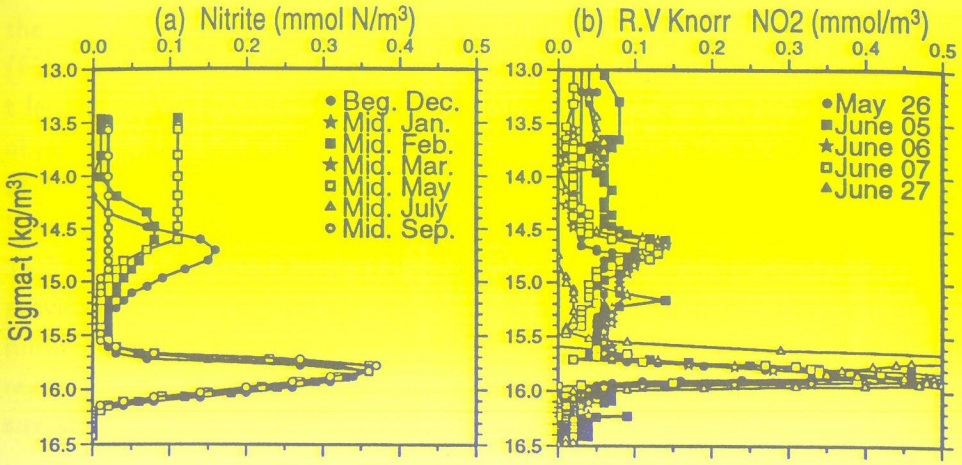

Figure 9: *(a) The model simulated daily averaged nitrite profiles versus density at selected times of the year, (b) the observed nitrite profiles versus density obtained by the R.V Knorr surveys in the Black Sea during summer 1988.*

peak is located within the oxygenated part of the water column at the same depths of the ammonium since the nitrite is an intermediate product of the NH_4 to NO_3 oxidation process. Presence of such peaks near the base of the euphotic zone with concentrations of about 0.2 mmol/m^3 are reported by Codispoti et al., (1991) and Basturk et al., (1994) and is also indicated in Fig. 9b. The second peak with concentrations of about 0.4 mmol/m^3 is developed within the suboxic layer near the 15.90 sigma-t level and is originated from its production during the nitrate reduction process. This peak therefore marks the begining of the denitrification which coincides in our model with the oxygen concentrations less than 3 μM. The position of this peak, however, shifts upwards by $\sim$0.05 kg/m^3 during the course of the year in response to H_2S-O_2 interactions within the suboxic layer. Fig. 9b shows that its location and magnitude are generally in agreement with the observational findings.

3.3. WATER COLUMN OXYGEN STRUCTURE

The vertical oxygen profiles shown in Fig. 10 indicate that the euphotic layer oxygen concentrations vary seasonally within a broad range of extremum values from 200 to 450 μM. The winter profiles (mid-December, end-January,

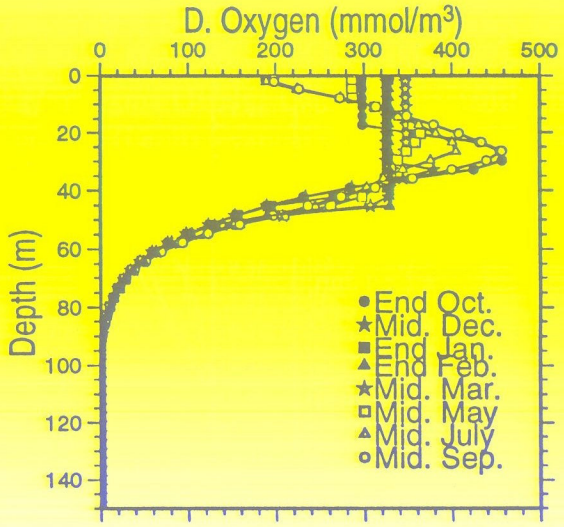

Figure 10: *The model simulated daily averaged dissolved oxygen profiles versus depth at selected times of the year*

end-February and mid-March) exhibit vertically uniform mixed layer concentrations of about 350 μM, ventilating at most the upper 50 m part of the water column as a result of the winter convective overturning process. The role of atmospheric oxygen input in the ventilation process depends upon the excess of the saturated oxygen over the surface oxygen concentrations (see eq. 23). The maximum contribution of oxygen saturation is realized towards the end of February during the period of coolest mixed layer temperatures (see Oguz et al., 1996, 1997), coinciding with the maximum and deepest winter oxygen concentrations during the year (Fig. 10). After March, once the cooling season comes to the end, the surface oxygen flux changes its sign implying loss of oxygen to the atmosphere during the spring and summer months. The signature of this loss in Fig. 10 is the reduction of the surface concentrations down to 200 μM in the summer. A linear trend of increase across the seasonal thermocline links them to the higher sub-thermocline oxygen concentrations. Depending on the strength of summer phytoplankton productivity, the sub-thermocline concentrations vary from 350 μM in mid-May to 450 μM during July and October at the times of flagellate blooms. Both the form of the euphotic layer oxygen structures and the range of variability of the oxygen concentrations agree well with the observations.

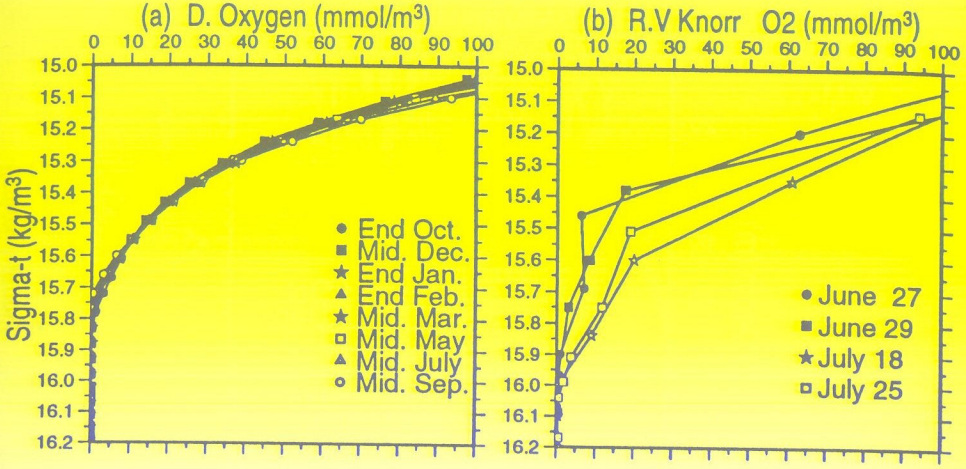

Figure 11: *(a) The model simulated daily averaged dissolved oxygen profiles versus density within the oxycline and suboxic layers at selected times of the year, (b) the observed dissolved oxygen profiles versus density obtained by the R.V Knorr surveys in the Black Sea during summer 1988.*

No major seasonal variations take place below 50 m. Irrespective of the seasons, the oxygen concentration decreases almost linearly within the oxcline zone to about 50 μM at 60 m, to 10 μM at 80 m, and vanishes at about 90 m (Fig. 10). Remineralization appears to be the major sink of oxygen at these levels, exceeding the oxygen consumption in the nitrification by almost an order of magnitude. The position of 10 μM oxygen concentrations corresponds roughly to the 15.6 sigma-t level, whereas the zero oxygen concentrations occur near the 15.8 sigma-t level (Fig. 11a). These model predictions on the position and slope of the oxycline zone, as well as its structure within the suboxic layer agree reasonably well with the available observations (Fig. 11b), even though the July data in Fig. 11b provide a slightly higher suboxic layer oxygen concentrations. As shown below, a slightly higher choice of the value of the vertical eddy diffusivity in the model can account for such variations.

Fig. 12 shows that the oxygen limitation function defined by eq. 12 reveals a step-like vertical structure throughout the year without possessing any seasonal variability. Its form implies almost no oxygen limitation on the remineralization and nitrification processes within the euphotic layer. On the other hand, a

strong control exits on the efficiency of these processes within the oxycline and the suboxic layer which are confined to a depth range between approximately 15.0 and 16.0 kg/m^3 sigma-t levels. The two characteristic features of the oxygen limitation function (i.e. its seasonal uniformity and simple step-like vertical structure) make possible to use it diagnostically in the Black Sea biochemical models if the oxygen is not a primary concern as a prognostic variable.

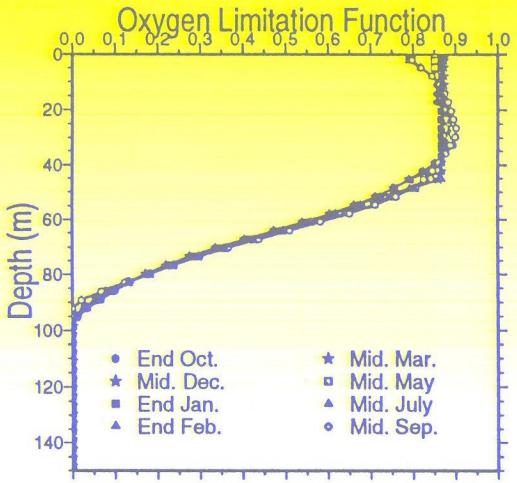

Figure 12: *The profiles of the dissolved oxygen limitation function computed according to eq.12 at selected times of the year*

Because the H_2S layer is located only about 100 m below the surface in most parts of the Black Sea, the possible vertical extention of the ventilation of the upper layer water column is a critically important issue. Apart from possible lateral ventilation events across the shelf break, one possible vertical ventilation mechanism is the convective overturning process following intense winter atmospheric cooling episodes. Although this process in general takes place intermittently in the form of strong cold air outbreaks, its role is studied in this model by specifying a smoothly varying, continuous but stronger cooling for the winter season. Then, using the equilibrium solution of the experiment described above as the initial condition, we force the model for one additional year with a three times stronger climatological heat flux (i.e. cooling) during the December-February period. Accordingly, the monthly averaged heat fluxes applied in this period are taken as 450, 390, 210 W/m^2. When compared with

the typical climatological conditions, the minimum winter mixed layer temperature is reduced to 2° C which is about 4.5° C lower than that of the standard run (see Fig. 3 in Oguz et al., 1996). Because of the presence of very strong upper layer stratification, this artificially high, season-long cooling causes only ~0.5 kg/m^3 increase in the mixed layer density. The corresponding mixed layer deepening is therefore insignificant and not more than about 7 m (Fig. 13a). Thus, it appears that the strong stability of the water column (Fig. 13b) hardly allows any seasonal variability of the oxygen below 50-60 m due to atmospheric ventilation. The intensified cooling, on the other hand, leads to an extra 40 μM increase in the winter mixed layer oxygen concentrations.

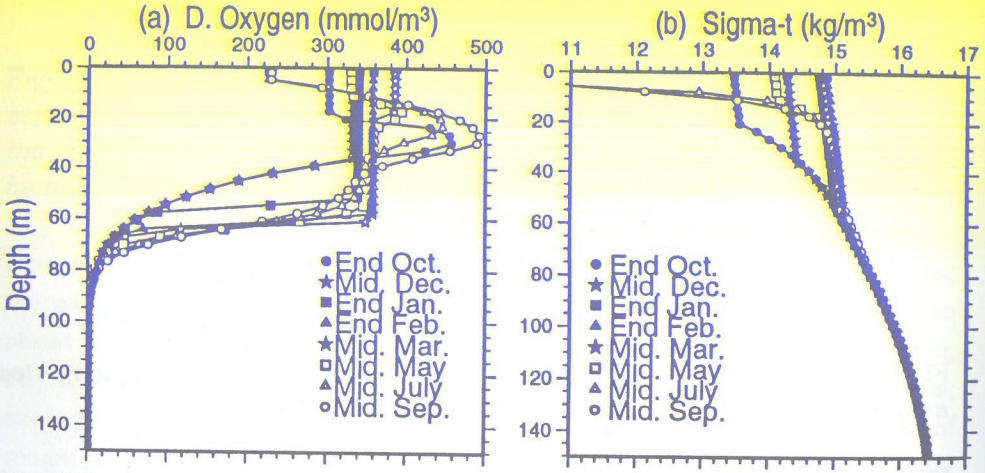

Figure 13: *The model simulated daily averaged (a) dissolved oxygen and (b) sigma-t profiles at selected times of the year for the case of stronger winter cooling*

The energetic internal wave-induced vertical mixing taking place in the vicinity of the oxycline region may contribute to the ventilation of the SOL. This possibility is demonstrated in Fig. 14 by taking ν_b=5.0x10^{-6} m^2/s at depths below 75m, instead of its standard value of ν_b=2.0x10^{-6} m^2/s. This new value results in higher oxygen concentrations within the entire oxycline with ~30 μM at the 15.6 sigma-t level and 10 μM around the 16.0 sigma-t level. The 2.0 μM oxygen concentration can even be traced at the 16.2 sigma-t level. It is however noteworthy to point out here that this structure is developed independently from its consumption during the H_2S oxidation.

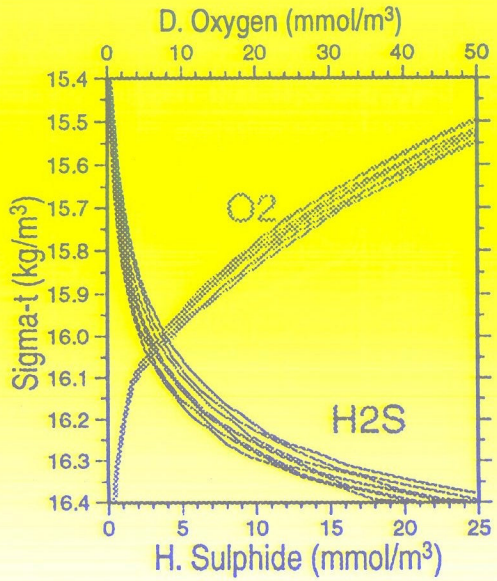

Figure 14: *The model simulated daily averaged dissolved oxygen profiles at every month of the year for the case of stronger vertical diffusivity within the oxycline and suboxic layers*

Possibility of this type of ventilation process remains to be validated by the data. The validation is however hampered by the difficulty that the relatively high oxygen values observed below the 15.6 sigma-t level are always questionable in the existing data. It is not always possible to distinguish whether or not such concentrations are a genuine feature or an artifact of the atmospheric contamination during the sampling.

3.4. SUBOXIC LAYER STRUCTURE

For the last numerical experiment, in the absence of H_2S oxidation by the oxygen and nitrate, the H_2S vertical structure developed as a result of the diffusive transport from the prescribed bottom source is shown in Fig.14 during the fourth years of model integration. The gradient zone established near the bottom boundary differs from the observations (e.g. see Murray et al., 1995) in such a way that, contrary to the trace level concentrations (~0.1 μM) above the 16.2 sigma-t level, our experiment reveals the values of about 5 μM near the anoxic interface decaying exponentially toward zero near the σ_t ~ 15.6 level. This structure resembles the co-existence layer claimed to be a real

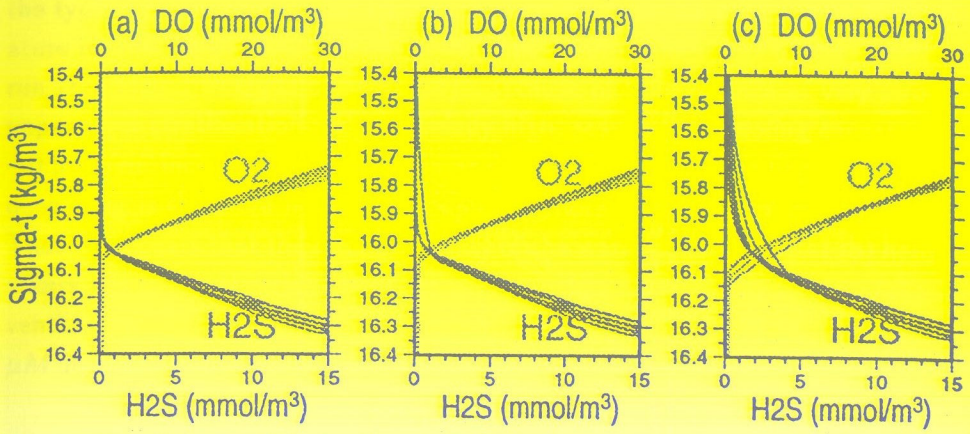

Figure 15: *The model simulated daily averaged dissolved oxygen and hydrogen sulphide profiles for the case of stronger vertical diffusivity within the oxycline and suboxic layers. These profiles show the evolution of the O_2-H_2S structure shown in Fig. 14 at selected times of the next year of integration after the H_2S oxidation by oxygen and nitrate is allowed in the model using (a) $\Omega_o = 0.1 day^{-1}$, (b) $\Omega_o = 0.05 day^{-1}$, (c) $\Omega_o = 0.01 day^{-1}$*

feature of the Black Sea upper layer biogeochemical structure (Faschuk et al., 1990).

It might be instructive to study further the evolution of this O_2-H_2S structure after the oxidation of H_2S by O_2 and NO_3 is allowed in the model. Hence, using the O_2-H_2S structure shown in Fig. 14 as the initial condition, the model is integrated one more year in order to demonstrate whether or not the oxygen and H_2S can exist together when they interact chemically. Fig. 15 shows three possible SOL structures for three different oxidation rates during the one year of model integration. In the case of $\Omega_n = 0.1$ day^{-1}, the entire H_2S within the SOL is oxidized rapidly within a few weeks (Fig. 15a). H_2S remains present only at depths where the oxygen and nitrate are no longer available for its oxidation (i.e. below $\sigma_t \sim 16.05$ level). When $\Omega_n = 0.05$ day^{-1}, the complete oxidation process takes longer than a month (Fig. 15b), after which a similar structure is developed. On the other hand, for the choice $\Omega_n = 0.01$ day^{-1}, the oxidation process proceeds very slowly and cannot deplete the whole H_2S in the suboxic layer within the year (Fig. 15c). At the end of the year, a C-layer type structure still persists with the presence of less than 2 μM H_2S concentrations within the SOL. Considering the fact that the typical H_2S oxidation rate suggested

by the measurements is about 0.1 day^{-1} (Jorgensen et al., 1991), the latter case should be regarded as the most unrealistic simulation. These numerical experiments therefore suggest that H_2S and O_2 cannot exist together since the fast reaction rate of the oxidation process will quickly deplete the H_2S. At most, H_2S can penetrate up to a level of vanishing oxygen concentrations.

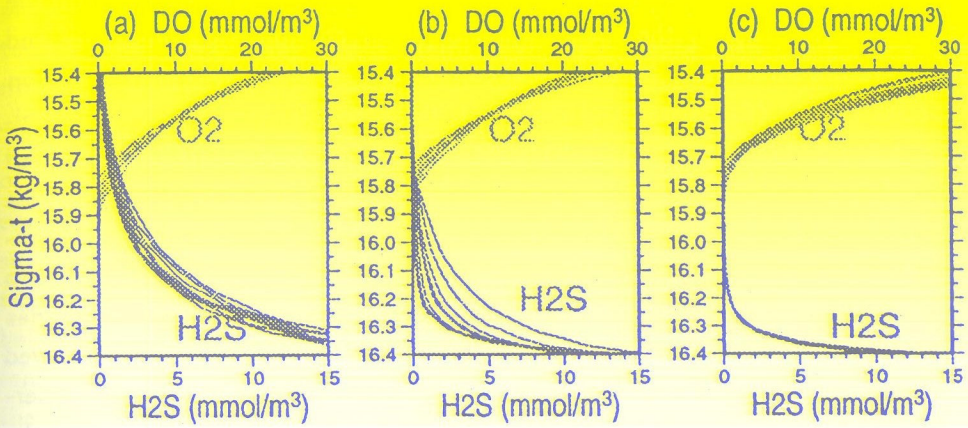

Figure 16: *The model simulated dissolved oxygen and hydrogen sulphide profiles within the oxycline and suboxic layers. These profiles show the evolution of the O_2-H_2S structure shown in Fig. 11 (a) within the third years of integration in the absence of the oxygen-sulphide interactions, and (b) within the subsequent year of integration after the H_2S oxidation by oxygen and nitrate is allowed in the model using $\Omega_o = 0.1 day^{-1}$ and $\Omega_s = 0.015 day^{-1}$, (c) during the following year of integration*

Similarly, for the case of the vertical oxygen structure shown previously in Fig. 11a, the evolution of the hydrogen sulphide structure as a result of vertical diffusive transport is shown in Fig. 16a within the fourth year of integration. For this case, the oxygen and H_2S overlapping layer is much narrower and is quickly eroded once the oxidation of the H_2S with the dissolved oxygen and NO_3 is allowed in the model using the respective oxidation rates of 0.1 and 0.015 day^{-1}. As shown in Fig. 16b, the oxygen and H_2S profiles are separated from each other gradually within the year. During the next year of time integration, an anoxic-nonsulfidic layer is finally established between 15.65 and 16.10 sigma-t levels (Fig. 16c), which resembles the SOL inferred from the observations. Incorporation of the Mn and Fe cycles near the anoxic interface should further contribute to the depletion of H_2S between the 16.1 and 16.2 sigma-t levels as implied by the observations.

4. Summary and Conclusions

The present paper describes an overview of our recent efforts on the simulation of upper layer biogeochemical structure in the central Black Sea using a one dimensional vertically-resolved coupled physical-biochemical modeling approach. The physical model involves the mixed layer dynamics, and is coupled with the biochemical model by the specification of water column eddy diffusivity and temperature structures. Its biological component considers two phytoplankton species groups (flagellates and diatoms), three zooplankton size groups (micro, meso and macrozooplankton), bacterioplankton, particulate and dissolved organic materials. The macrozooplankton group identifies a particular species group called the medusae "Aurelia aurita" which dominated the ecosystem during 80's prior to the population explosion of another gelatinous carnivore group called "Mnemiopsis leidyi". The chemical component of the model includes the equations for the ammonium, nitrite, nitrate as well as for the dissolved oxygen and hydrogen sulphide. The model is therefore able to represent different biochemical processes interacting with each other in different parts of the water column, and therefore allows a dynamical coupling between the euphotic zone, the oxycline/upper nitracline layer, and the suboxic and the anoxic layers. However, the full redox processes which we think to take place across the suboxic-anoxic interface have not been incorporated in this model yet. This is a work in progress and will be reported elsewhere later.

Given a set of parameters, the model is shown to provide a reasonably adequate representation of the basic features of the biogeochemical structure consistent with the observations. The results of the simulations on the living component of the biological model are compared with the composite data gathered within the last two decades by the Shirshov Institute of Oceanology. The data collected during the Knorr 1988 surveys are used primarily to validate the results of the chemical component of the model.

The model produces three diatom blooms during March, late May-early June and December, whereas flagellates dominate the system during most of the summer and the entire autumn, starting from the end of June to the begining of November. This yearly phytoplankton structure possesses more pronounced bloom characteristics during summer months as compared with the previous

model described in Oguz et al. (1997), and may point out the role of gelatinous carnivores started dominating the ecosystem during 1980's. This is due to a new "top-down" control in the food web structure in which increasing the gelatinous carnivore population put a stronger control on the mesozooplankton community which subsequently weakens their grazing pressure on the phytoplankton structure. The most pronounced signature of this effect is observed towards the end of May and September which coincide with the periods of major increase in the Medusae population.

The model allows the coupled nitrogen-oxygen dynamics via the specification of oxygen-dependent nitrification and remineralization rates. The oxygen, generated photosythetically and by the ocean-atmosphere interactions at the near-surface levels, are consumed during the organic matter decomposition and nitrification at subsurface levels which normally reveal very restricted ventilation below 50 m in the central Black Sea away from the shelf and the Rim Current frontal regions. Below the euphotic zone, the vertical oxygen structure therefore undergoes very steep variations with almost two order of magnitude changes in their concentrations within about 25 m interval (oxycline). Typically, the $\sim$10 μM oxygen level identifies the position of vanishing aerobic mineralization and nitrification processes in the water column. The oxycline thus coincides with strong nitrate variations (upper nitracline) in which the nitrate concentrations increases from their trace level values in the mixed layer up to the maximum values of 6-8 μM across this zone.

In the oxygen deficient part of the water column (i.e. $O_2 < 10\mu M$), the organic matter decomposition occurs via the denitrification process. This causes excessive nitrate consumption within a narrow layer adjacent to the oxycline and associated strong reduction in the nitrate concentrations. A distinguishing signature of the denitrification in the model is the formation of a narrow nitrite peak located at about 15.8-15.9 sigma-t levels. Between the two nitracline zones with opposite slopes, the nitrate concentrations exhibit a maximum, whose position is intimately related with the location of the onset of the trace level oxygen concentrations as they control the lower limit of the nitrification and the onset of the denitrification in the water column. Its position corresponds approximately to the sigma-t levels of 15.4-15.6 kg/m^3, below which the layer extending up to the depth of 16.2 sigma-t level is called the suboxic layer to emphasize its oxygen deficient and nonsulfidic characters.

The additional nitrate consumption takes place near the anoxic interface for oxidizing the hydrogen sulphide. This appears to be the primary mechanism maintaining the hydrogen sulphide-free suboxic layer. The oxidation of H_2S by metal oxides, which was believed to be the main oxidation process up to now, should therefore be a secondary importance whereas it might have some contributions at depths below the vanishing nitrate concentrations. The numerical experiments suggest that the lower boundary of the suboxic zone has a fairly stable character, and is identified near the 16.1 sigma-t level. The position of its upper boundary, on the other hand, may undergo significant variations depending on the ventilation characteristics of the subsurface levels. As an extreme case, the positions of the vanishing sulphide and oxygen concentrations may coincide with each other, and the thickness of SOL goes to zero but they are never overlapped in any case. They therefore imply that the layer of co-existence of the oxygen and hydrogen sulphide is not possible because of the fast reaction rate of the oxidation mechanism and therefore should be an artifact of the measurements.

The manganese cycling is proposed to play a catalytical role on the ammonium and sulphide oxidation (Murray et al., 1995). According to this hypothesis, both NH_4 and H_2S are oxidized by MnO_2 to produce N_2 and Mn^{++}, the latter of which interacts subsequently with NO_3 to procude MnO_2 once again. This mechanism might explain how trace level ammonium and hydrogen sulphide concentrations are maintained near the anoxic interface at the expense of the continual nitrate consumption at these levels. This mechanism further suggests that the nitrate loss must be compansated by its downward diffuse flux from the upper part of the SOL near the nitrate peak and/or quasi-lateral inputs due to excessive antropogenic load from rivers. Otherwise, a gradual rise of the position of trace level nitrate concentrations near the anoxic interface should take place in time. This point, however, remains to be verified by further modeling and observational studies.

Acknowledgements

This work was carried out within the scope of the TU-Black Sea Project sponsored by the NATO Science for Stability Program. It is supported in part by the National Science Foundation Grant OCE-9633145. A partial support was also provided by the Turkish Scientific and Technical Research Council (TUBITAK). We wish to thank M.E. Vinogradov for his continual support and valuable comments.

References

Basturk, O., C. Saydam, I. Salihoglu, L. V. Eremeeva, S. K. Konovalov, A. Stoyanov, A. Dimitrov, A. Cociasu, L. Dorogan, M .Altabet (1994) "Vertical variations in the principle chemical properties of the Black Sea in the autumn of 1991". J. Marine Chemistry, 45, 149-165.

Basturk, O., S. Tugrul, S. Konovalov, I. Salihoglu (1997) "Variations in the vertical structure of water chemistry within the three hydrodynamically different regions of the Black Sea". In: Sensitivity to change: Black Sea, Baltic Sea and North Sea, E. Ozsoy and A. Mikaelyan (Editors), NATO ASI Series 2. Environment- Vol. 27, 183-196.

Broecker, W.S. and T.H. Peng (1982) "Tracers in the sea". Eldigo Press, Lamont- Doherty Geological Observatory, Palisades, 690 pp.

Buesseler,K.O., H.D. Livingston, L.Ivanov, A. Romanov (1994) "Stability of the oxic-anoxic interface in the Black Sea". Deep Sea Research, 41, 283-296.

Codispoti, L.A., G.E. Friederich, J.W. Murray, and C. M. Sakamoto (1991) "Chemical variability in the Black Sea: implications of continuous vertical profiles that penetrated the oxic/anoxic interface". Deep Sea Res., 38, Suppl 2, S691-S710.

Eremeev, V.N. (1996) "Hydrochemistry and dynamics of the hydrogen-sulphide zone in the Black Sea". Unesco reports in marine Science, Ed. by R.C. Griffiths, Unesco 1996, 114 pp.

Faschuk,D.Ya., T.A. Ayzatullin, V.V. Dronov, T.M. Pankratova, M.S. Finkelshteyn (1990) " Hydrochemical structure of the layer of coexistence of oxygen and hydrogen sulphide in the Black Sea and a possible mechanism of its generation". Oceanology (English transl.), 30, 185-192.

Gargett, A.E. (1984) "Vertical eddy diffusivity in the ocean interior". J. Marine Research, 42, 359-393.

Jorgensen, B.B., H. Fossing, C.O. Wirsen, H.W. Jannasch (1991) "Sulfide oxidation in the anoxic Black Sea chemocline". Deep Sea Reseach, 38, suppl.2, S1083-S1103.

Lebedeva, L.P., and E.A. Shushkina (1991) "Evaluation of population characteristics of the medusae *Aurelia aurita* in the Black Sea. Oceanology (English transl.), 31, 314-319.

Lewis,L.B. and W.M. Landing (1991) "The biogeochemistry of manganese and iron in the Black Sea". Deep Sea Reseach, 38, suppl.2, S773-S803.

Lipschultz, F., S.C.Wofsy, B.B.Ward, L.A.Codispoti, G. Friedrich, J.W. Elkins (1990) "Bacterial transformations of inorganic nitrogen in the oxygen-deficient waters of the Eastern Trophical South Pacific Ocean". Deep Sea Research, 37, 1513-1541.

Murray, J.W., H. W. Jannash, S. Honjo, R. F. Anderson, W.S. Reeburgh, Z. Top, G.E. Friederich, L.A. Codispoti, E. Izdar (1989) "Unexpected changes in the oxic/anoxic interface in the Black Sea". Nature, 338, 411-413.

Murray, J.W., L.A. Codispoti, G.E. Friederich (1995) "Oxidation-reduction environments: The suboxic zone in the Black Sea". In: Aquatic chemistry:Interfacial and interspecies precosses. ACS Advances in Chemistry Series No.224. C.P. Huang, C.R.O'Melia, and J.J. Morgan (Editors), 157-176.

Olesen, N.J., K. Frandsen, H.U. Riisgard (1994) "Population dynamics, growth and energetics of jellyfish *Aurelia aurita* in a shallow fjors". Mar. Ecology Prog. ser., 105, 9-18.

Oguz,T., P. Malanotte-Rizzoli, D. Aubrey (1995): "Wind and Thermohaline circulation of the Black Sea driven by yearly mean climatological forcing". J. Geophysical Research, 100, 6845-6863.

Oguz, T. and P. Malanotte-Rizzoli (1996) "Seasonal variability of wind and thermohaline driven circulation in the Black Sea: Modeling studies". J. Geophysical Research, 101, 16551-16569.

Oguz, T., H. Ducklow, P. Malanotte-Rizzoli, S. Tugrul, N. Nezlin, U. Unluata (1996) "Simulation of annual plankton productivity cycle in the Black Sea by a one-dimensional physical-biological model". J. Geophysical Research, 101, 16585-16599.

Oguz, T., H. Ducklow, P. Malanotte-Rizzoli, J.W. Murray V.I. Vedernikov, U. Unluata (1997) "A physical-biochemical model of plankton productivity and nitrogen cycling in the Black Sea". to appear in Deep Sea Research.

Rozanov, A.G. (1996) "Redox stratification in Black Sea waters". Oceanology

(English transl.), 35, 500-504.

Samodurov, a.S., A.A. Lyubitsky, N.A. Pantaleev (1994) "A contribution of the overturning internal waves to the structures, energy dissipation and vertical diffusion in the ocean. Mar. Hydrophysical Journal, 3,, 14-27.

Saydam, C., S. Tugrul, O. Basturk, T. Oguz (1993) "Identification of the oxic/anoxic interface by isopycnal surfaces in the Black Sea". Deep Sea Research, 40, 1405-1412.

Shushkina,E.A., and E.I. Musayeva (1983) "The role of jellyfish in the energy system of the Black Sea plankton communities". Oceanology (English transl.), 23, 92-96.

Shushkina,E.A., and E.I. Musayeva (1990) "Structure of planktic community of the Black Sea epipelagic zone and its variation caused by invasion of a new ctenophore species". Oceanology (English transl.), 30, 225-228.

Tugrul, S., O. Basturk, C. Saydam, A. Yilmaz (1992) "The use of water density values as a label of chemical depth in the Black Sea". Nature, 359, 137-139.

UNESCO (1986) "Progress on oceanographic tables and standards 1983-1986: work and recommendations of the UNESCO/SCOR/ICES/IAPSO Joint Panel. Unesco Techn. Pap. Mar. Sci., 50, 50pp.

Vedernikov, V.I. and A.B. Demidov (1997) Vertical distribution of primary production and chlorophyll during different seasons in deep regions of the Black Sea. Oceanology (English transl.), 37, 376-384.

Vinogradov, M.E., and Yu.R. Nalbandov (1990) "Effect of changes in water density on the profiles of physicochemical and biological characteristics in the pelagic ecosystem of the Black Sea". Oceanology (English trans.), 30, 567-573.

Vinogradov, M.E. and E.A. Shushkina (1992) "Temporal changes in community structure in the open Black Sea". Oceanology (English transl.), 32, 485-491.

Walsh, J.J. and D.A. Dieterle (1984) "CO_2 cycling in the coastal ocean. I - A numerical analysis of the southern Bering Sea with applications to the Chukchi Sea and the northern Gulf of Mexico". Prog. Oceanogr., 34, 335-392.

Yakushev,E.V. and L.N. Neretin (1997) "One dimensional modeling of nitrogen and sulfur cycles in the aphotic zone of the Black and Arabian Seas". to appear in J. Global Biogeochemical Cycles.